SIMULATION OF SEAKEEPING TESTS USING OPENFOAM

Jan Löhrmann*
Technical University of Berlin
Department of Dynamics of Maritime Systems
Berlin, Germany
Email: jan-patrick.loehrmann@tu-berlin.de

Andrés Cura Hochbaum
Technical University of Berlin
Department of Dynamics of Maritime Systems
Berlin, Germany

INTRODUCTION

In the past, seakeeping analysis has almost solely been done using potential theory based methods. As long as pressure dominated effects are analysed, these methods yield good accuracies with very low computational effort. However, if viscous effects can't be neglected these methods can no longer be applied. As the development of viscous flow solvers took place rapidly and computational resources became cheaper, the application of RANS solvers onto difficult unsteady situations became more and more practicable.

This study has been done to validate the open source code *OpenFoam* for such cases. The benchmark ship DTMB 5415 was used for this purpose, which has been investigated for many years e.g. in the CFD Workshop Tokyo 2005 [1]. The model's dimensions are listed in table 1. Validation was done for two test cases, namely calm water and head waves. Afterwards, further simulations were performed for a sea spectrum analysis. The conditions for the two test cases are listed in table 2.

TABLE 1. MAIN PARTICULARS OF THE DTMB 5415

L_{PP}	5.72 m	Length btw. perp.
B	0.768 m	Breadth
T	0.248 m	Draught
S_0	4.861 m^2	Wetted surface
t_{FP}	-0.017732 m	Trim fwd. perp.
t_{AP}	-0.004 m	Trim aft. perp.

NUMERICAL METHOD

Two solvers were used for the simulations.*interFoam* was used to simulate the calm water condition. *interFoam* is a standard solver within *OpenFoam* for incompressible multiphase flows, where the interface is being solved by using the Volume of Fluid method. The equations which are solved are the Reynolds averaged Navier-Stokes equations (RANSE) in combination with the continuity equation for incompressible fluids. Coupling of pressure and velocity is done using the PISO algorithm. The turbulence has been modelled using the k-ω-SST model based on [2]. Since a fixed trim has been prescribed, no ship movements had to be investigated.

TABLE 2. TEST CASE CONDITIONS

Test case "Calm Water"		
v	2.1 m/s	Ship velocity
Fr	0.28	Froudenumber
Re	1.201E+07	Reynoldsnumber
Test case "Head Waves"		
v	2.1 m/s	Ship velocity
$\lambda = 1,5 \cdot L_{PP}$	8.58 m	Wave length
$A_k = 2 \cdot \pi \cdot \zeta / \lambda$	0.025	Wavesteepness
ζ_a	0.034 m	Amplitude
ω_e	4.2179 rad/s	Encountering freq.

waveFoam was the second solver used for the simulations of the ship in waves. This solver is based on *interFoam* with several additions to e.g. generate different wave types. Furthermore, relaxation zones have been implemented to generate and absorb the waves and avoid reflections. This relaxation technique is achieved by applying a relaxation function (Eqn. (1)) in the defined zones to influence the computation of the velocity field and the phase fraction (Eqn. (2)).

$$w = 1 - \frac{exp(\sigma^p) - 1}{exp(1) - 1} \quad \text{for} \quad \sigma \in [0;1] \tag{1}$$

$$\phi = (1 - w)\phi_{target} + w \cdot \phi_{computed} \tag{2}$$

where σ is 0 in the free computational domain (around the ship) and increases linearly to 1 at the do-

*Address all correspondence to this author.

main boundaries at the inlet and outlet. The exponent p can be chosen and is set to 3.5 as default value. Full descriptions of the solver can be found in [3].

Grid Dependency

Grid generation has been done using the commercial software *Hexpress*, which produces unstructured, full-hexahedral meshes. The dynamic trim of the ship has already been considered while generating the grid. Four different grids were generated using a grid refinement ratio of $r_G = 2$ to perform a grid analysis. The grid size as well as the cells per wave length λ and height H are shown in table 3. The x-axis of the grid is directed along the untrimmed longitudinal axis of the ship, the y-axis is directed positive to starboard and the z-axis is directed positive upwards. Grid dependency has been investigated on both test cases. Symmetry was assumed at the central-longitudinal plane. The non-dimensional wall distance y^+ has been chosen to be about 80 combined with using wall functions [4]. Table 4 shows the total resistance and its frictional and pressure components for the four grids at a time step of $\Delta t = 0.001$. The results show an acceptable convergence with the exception of a slight increase of the resistance at grid 1. The convergence ratio for the total resistance F_x for the grids 1-3 and grids 2-4 are defined according to [5]:

TABLE 3. NUMERICAL GRIDS

Grid #	Cells	z/H	x/λ
1	11.650.000	11	294
2	1.600.000	10	146
3	300.000	8	73
4	73.000	6	37

TABLE 4. GRID DEPENDENCY FOR CALM WATER

Grid #	F_x [N]	F_F [N]	F_P [N]
1	23,97	16,44	7,53
2	22,30	15,83	6,47
3	26,79	15,69	10,83
4	35,81	13,62	22,18

$$R_{i,1-3} = \frac{\varepsilon_{i,21}}{\varepsilon_{i,32}} = \frac{\hat{S}_{i,2} - \hat{S}_{i,1}}{\hat{S}_{i,3} - \hat{S}_{i,2}} = -0,37 \qquad (3)$$

$$R_{i,2-4} = \frac{\varepsilon_{i,32}}{\varepsilon_{i,43}} = \frac{\hat{S}_{i,3} - \hat{S}_{i,2}}{\hat{S}_{i,4} - \hat{S}_{i,3}} = 0,50 \qquad (4)$$

with $\hat{S}_i$ being the solution of the respective grids. The convergence ratio shows a monotone convergence for grids 2-4, while grids 1-3 only achieve an oscillatory convergence. The frictional resistance in grid 1 increases compared to grid 2 which leads to a divergence of the frictional resistance for grids 1-3.

Similar results were achieved for the test case of head waves with the addition that the wave amplitude ratio ζ_a/ζ shows a monotone convergence from 0.83 on grid 4, to 0.97 on grid 1, with ζ_a being the generated amplitude and ζ the target amplitude. Grid 2 already achieves 0.96. The generated amplitude has been determined through Fourier analysis of the free-surface elevation in the far field of the ship and averaging between the fore and aft perpendicular. All calculations were made with only one PISO iteration.

The residuals and the convergence of the resistance on grid 2 show a satisfactory behaviour while having a reasonable resolution with approximately 1.6 million cells. That was the reason why it was decided to use this grid for the further investigations.

Timestep Dependency

A time step dependency analysis has been performed for both test cases to determine the influence of the chosen time step on selected results. Time steps from $\Delta t = 5 \cdot 10^{-5}$ up to $1 \cdot 10^{-2}$ have been investigated.

Although grid 2 was selected in the previous section, it was decided to use grid 3 for the time step analysis, as the computational time was wanted to be kept reasonable even at very small time steps of up to $5 \cdot 10^{-5}$. Therefore, this analysis can only indicate qualitative but not quantitative trends. It has to be mentioned, that with the release of OpenFoam-2.3.0, a significant enhancement of the applicable time step due to an implementation of a semi-implicit solver for the phase fraction has been achieved. Simulations with the previous explicit version of the phase solver where restricted to Courant numbers < 1, which resulted in extremely high computational times. During the time step dependency analysis, a maximum Courant number, time-averaged between 10s - 20s simulation time of up to 30 was achieved without affecting the convergence.

Figure 1 shows the resistance coefficient c_T over the investigated time steps. It can be seen that there is a strong dependency on the time step. The resis-

tance coefficient increases dramatically with decreasing time step. The resistance coefficient is almost constant from $\Delta t = 0.001$ on towards bigger time steps.

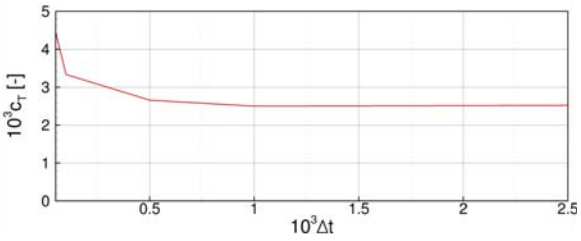

FIGURE 1. TIME STEP DEPENDENCY FOR CALM WATER CONDITION

Only three time steps have been investigated for the test case with head waves, as very high and very low time steps lead to divergence of the solution. Nevertheless, the time step dependency is similar to the calm water condition. This confirms that for each case considered a certain lower limit of Δt should be kept. In addition to the resistance, the generated wave amplitude has been investigated as well. The wave amplitude ratio ζ_a/ζ increases from 0.88 up to 0.94 when decreasing the time step one order of magnitude from $\Delta t = 0.005$ to $\Delta t = 0.0005$. Only small changes from $\Delta t = 0.001$ to $\Delta t = 0.0005$ could be seen, which is why it was decided to choose the time step $\Delta t = 0.001$ for all further calculations.

Influence of PISO Iterations

All calculations for the calm water test casewere done with only one PISO iteration, as this is a pseudo unsteady flow. One and four PISO iterations were tested for the test case with head waves. The resulting forces barely change when increasing the number of iterations. Nevertheless, more iterations strongly influence the quality of the achieved wave amplitude. The wave amplitude ratio ζ_a/ζ can be enhanced on grid 3 from 0.93 to 0.97 using four instead of one iteration. It has to be mentioned that stability problems occurred when starting with a higher number of PISO iteration.

RESULTS OF VALIDATION

Calm Water

The simulation was done using grid 2 at a time step of $\Delta t = 0.001$ and one PISO iteration. This resulted in a computational time of 103 hrs for 20s simulation time on 4 processors (Intel Xeon E5607 2.27GHz).

Figure 2 shows the total resistance (red) and its pressure (blue) and frictional component (green). The dotted line indicates the experimental value for the total resistance. The computed resistance is in a good agreement with the experimental data. The error E defined according to [5] is about 1.7%D. The free-

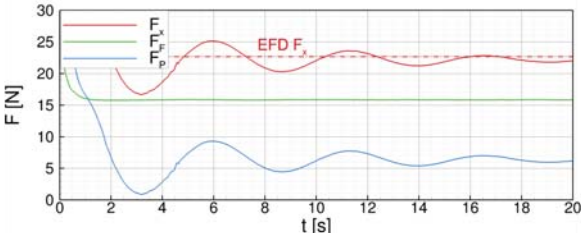

FIGURE 2. RESISTANCE FORCES FOR CALM WATER CONDITION

surface elevation can be seen in fig. 3. Compared to the experimental data shown on the top side, the simulation has a satisfactory agreement with slightly smaller amplitudes. This is due to numerical damping caused by a rather unfortunate strong expansion of the cell size in transverse direction. Further grid refinement, especially in regions further away from the hull, would lead to an enhancement of the achieved wave amplitude. However, this has not been considered in this investigation, since the focus lays on the simulation of seakeeping tests. The results of the calm water test have been considered as sufficiently satisfactory for this purpose.

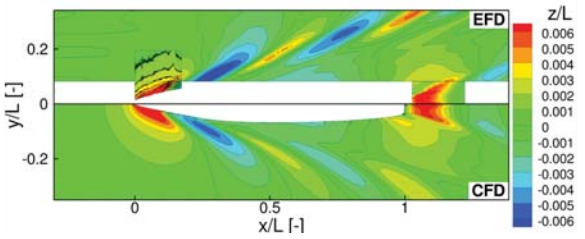

FIGURE 3. COMPARISON OF EXPERIMENTAL AND NUMERCIAL FREE-SURFACE ELEVATION FOR CALM WATER CONDITION

Head Waves

The simulation was done using grid 2 with a time step of $\Delta t = 0.001$. Only one PISO iteration has been done, as a wave amplitude ratio of 0.96 has already been achieved which is seen as sufficient. Further increasing of the PISO iterations would have lead to longer computational time but only fewer improvements as shown above. The computational time and time averaged maximum Courant number are very similar to the calm water test case.

Figure 4 shows the surface elevation at $x = 0$ (FP) in the far field, where no influence of the ship wave system occurs. The generated wave has a good agreement with the analytical solution with less than 5%

deviation in the wave amplitude. Furthermore, fig. 5

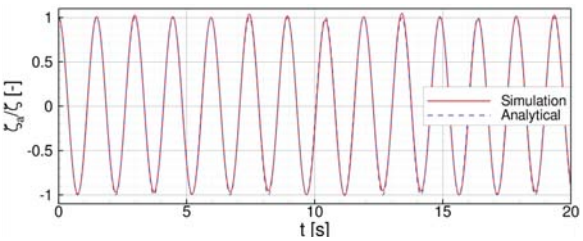

FIGURE 4. WAVE AMPLITUDE AT $x = 0$ (FP) IN THE FAR FIELD OF THE SHIP

shows the elevation of the wave amplitude over the domain at four instants namely $\frac{t}{T_e} = 0$, $\frac{1}{4}$, $\frac{2}{4}$ and $\frac{3}{4}$, with T_e being the encountering period of the wave which is defined to have a non-dimensional elevation of 1 at $x = t = 0$. It can be seen that the wave amplitude ratio resumes at a good level of around 1 and waves are being damped effectively by the relaxation zone at the outlet, which starts at $x/L \approx 1.9$. To analyse the resistance, the signal of the total force

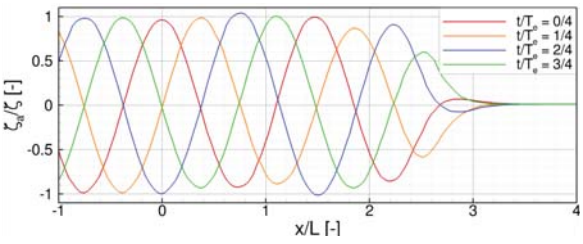

FIGURE 5. WAVE AMPLITUDE IN THE FAR FIELD OF THE SHIP AT FOUR DIFFERENT INSTANTS

component in longitudinal direction has been Fourier analysed (fig. 6). The plot visualises the 0th and 1st harmonics. The 0th harmonic has an amplitude of $\frac{a_0}{2} = 23.533N$ and represents the mean resistance in head waves. The 1st harmonic has an amplitude of 37.879 N and is the first order force due to the head waves of $f_e = 0.6713Hz$. The frequency of the signal has a good agreement with the generated encountering frequency of the wave. At $f/f_e = 2$ a multiple of the encountering frequency can be seen with a very low amplitude. Additionally, a local maximum at $f/f_e = 0.251$ with an amplitude of 1.02 N occurs. This local maximum can be explained by reflections of the waves at the domain boundaries. Nevertheless, the influence of these reflections is small compared to the amplitude of the 1st harmonic.

The resistance, dynamic buoyancy and pitching moment were made non-dimensional using equations 5. The comparison of the determined forces/moment (red) with the results of the flow code *Neptun*, which also participated in the CFD Workshop

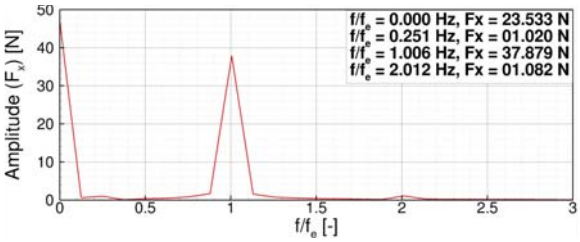

FIGURE 6. COMPONENTS OF THE FOURIER ANALYSIS OF THE TOTAL RESISTANCE OVER NON-DIMENSIONAL FREQUENCY

Tokyo 2005 [6] and the experimental data (blue) are shown in fig. 7. At first, a good agreement can be seen between the results of *OpenFoam* and *Neptun*. In both cases, the peak values don't always match the experimental data but are within a good correspondence. Moreover, a difference in the phase between the experimental data and both numerical data can be seen, which already occurred in the mentioned workshop and is most probably caused by a time lag in the experimental data.

$$c_T = \frac{F_x(t)}{\frac{\rho}{2} \cdot v^2 \cdot S_0}, \quad c_H = \frac{F_z(t)}{\frac{\rho}{2} \cdot v^2 \cdot S_0}, \quad c_M = \frac{M_y(t)}{\frac{\rho}{2} \cdot v^2 \cdot S_0 \cdot L_{PP}} \tag{5}$$

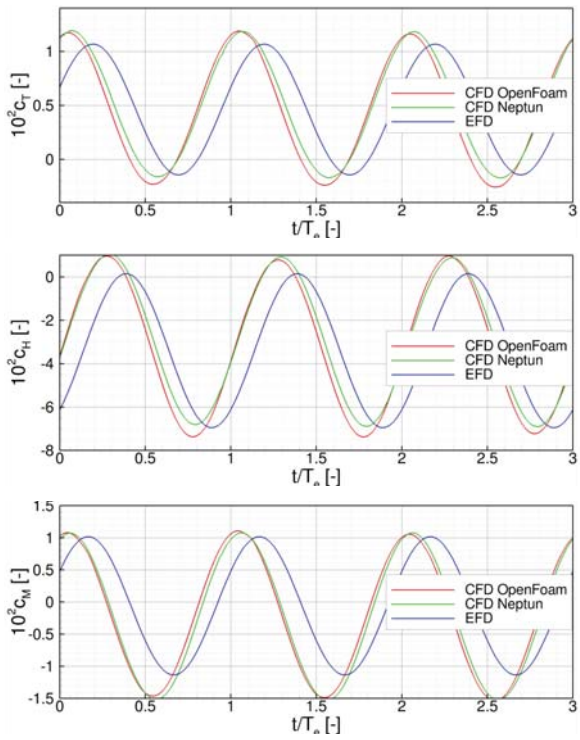

FIGURE 7. COMPARISON OF OPENFOAM, NEPTUN AND EXPERIMENTAL RESULTS FOR c_T, c_H AND c_M

SEA SPECTRUM ANALYSIS

After having validated the generation of regular waves, a sea spectrum was tested. The generation of sea spectra is already included in *waveFoam* but limited to standard spectra for ships at zero speed. A limitation of $0.5 \cdot f_P \leq f \leq 2 \cdot f_P$ was applied to exclude higher and lower frequencies (standard setting is $0.3 \cdot f_P \leq f \leq 3 \cdot f_P$). The same grid as before was used to generate a JONSWAP spectrum with the parameters, as shown in table 5. This leads to a surface elevation at $x = 0$ in the far field as shown in fig. 8.

TABLE 5. PARAMETERS OF THE JONSWAP SPECTRUM

H_S	0.2 m	Significant wave height
T_P	2.3441 s^{-1}	Peak period
γ	3.3	Peak enhancement factor
μ_0	180 °	Encountering angle
N	10	Number of frequencies

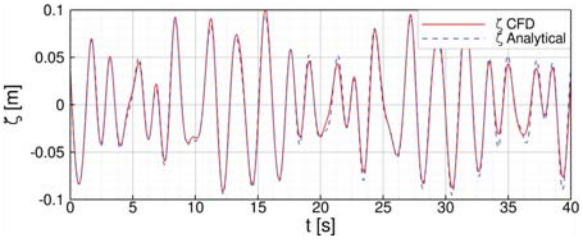

FIGURE 8. WAVE AMPLITUDE OF THE GENERATED WAVE SPECTRUM AT $x = 0$ (FP)

As with the regular waves, there is a good agreement between the analytical solution of the wave train and the generated waves. The deviation of the wave amplitude is less than 5% in the peaks for the first 20s of simulation time. This is increasing slightly to maximal 10% up to 40s simulation time.

Afterwards, the individual wave components, which were used to generate the spectrum, where simulated separately. Those waves are listed in table 6 with their respective non-dimensional amplitude $2 \cdot \zeta / H_S$, frequency f/f_P, the random chosen phase ε and the steepness $A_k = 2\pi \cdot \zeta / \lambda$. The accuracy of the individual wave amplitudes is shown in fig. 9 for 3 out of 10 wave components. The generated wave amplitudes are in general in a good agreement with the respective analytical solution from the 3rd wave onwards. Only waves number 1 and 2 are not very accurate in their amplitude and period. This can be explained by their low wave height, long wave length and consequently low steepness. Waves 3-10 have an average deviation of their wave amplitude of only 0.7%. Finally, the total resistance and wave amplitude of the single wave components have been superposed, as shown in figure 10. Not only the superposition of the wave amplitudes but also of the resistance of the single components agrees well with the corresponding signal of the wave spectrum simulation. This indicates that higher order forces are of less importance considering this particular spectrum. On the other hand, this indicates that the resistance of the ship due to several individual waves can be determined by generating a wave spectrum and analysing the resistance signal through Fourier analysis to determine the

TABLE 6. INDIVIDUAL WAVE COMPONENTS OF THE GENERATED SPECTRUM

Wave #	$2 \cdot \zeta / H_S$	f/f_P	ε	A_k
1	0.031005	0.575001	0.76095	0.0008
2	0.137892	0.725000	2.16132	0.0054
3	0.322803	0.875001	6.16261	0.0181
4	0.384560	1.025000	1.30606	0.0296
5	0.293996	1.175000	1.92987	0.0297
6	0.202895	1.325000	1.29352	0.0261
7	0.165854	1.475000	5.32802	0.0264
8	0.135921	1.625000	0.69639	0.0263
9	0.111905	1.775000	4.06245	0.0258
10	0.092901	1.925001	2.41405	0.0252

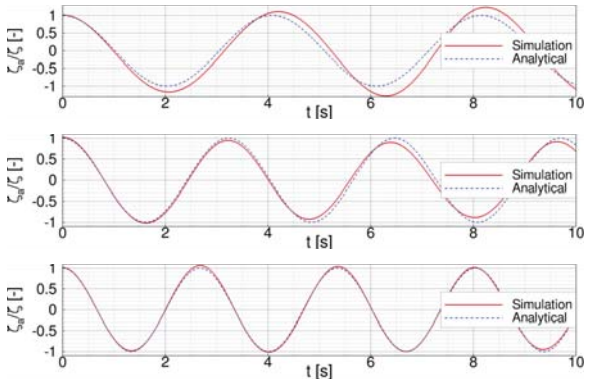

FIGURE 9. FIRST THREE WAVE AMPLITUDES OF THE INDIVIDUAL COMPONENTS OF THE SPECTRUM AT $x = 0$ (FP)

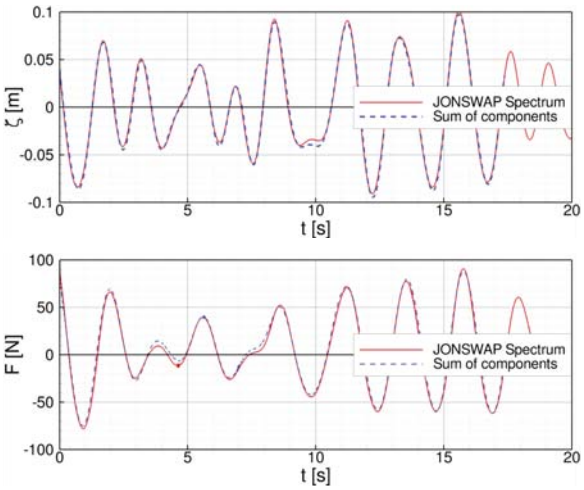

FIGURE 10. COMPARISON OF THE WAVE AMPLITUDE (TOP) AND RESISTANCE (BOTTOM) OF THE WAVE SPECTRUM SIGNAL (RED) AND THE SUPERPOSITION OF THE WAVE COMPONENTS (BLUE)

TABLE 7. 1st HARMONICS OF THE SIGNAL OF THE SINGLE WAVE COMPONENTS AND THE SPECTRUM

f [Hz]	F_x [N] Single wave	F_x [N] Spectrum	E [%D]
0.245297	1.847	2.745	-49 %
0.309287	11.895	13.913	-17 %
0.373278	29.211	24.257	+17 %
0.437268	36.193	31.700	+12 %
0.501258	22.603	21.416	+5%
0.565249	9.696	10.765	-11%
0.629239	3.287	4.463	-36%
0.693230	2.284	2.913	-22%
0.757220	1.996	2.113	-6%
0.821211	0.940	0.963	-2%

respective resistance for each wave. Fourier analysis has been done for the wave spectrum signal and all individual waves . Tab. 7 contains the determined first harmonics of each individual wave component as listed in tab. 6 as well as of the spectrum signal. The error E indicates the deviation of the force amplitudes at the respective frequencies in the spectrum from the force amplitudes of the individual wave components. The magnitude of the force amplitudes of the wave spectrum differs up to 49% from the force amplitudes of the individual wave components. This concerns mainly the frequencies at the boundaries of the spectrum, which are having small amplitudes. However, the amplitudes of the wave components with the highest energy of the spectrum can be predicted with $\pm$17%. It has to be noted, that a signal with 40s simulation time has been used for the Fourier analysis of the spectrum, instead of the shown signal of 20s simulation time (see fig. 10). This yields a much better agreement with the Fourier analysis of the single wave components as with the signal with only 20s simulation time.

CONCLUSION

It has been shown, that *OpenFoam* in combination with *waveFoam* is capable of producing good results regarding the accuracy of wave amplitude and length of regular and irregular seas. Waves with a low steepness are of less accuracy, which is due to numerical damping. The influence of wave reflections is low and the efficiency of the absorbing zones is good. The comparison of the resulting forces with experimental data shows a good agreement, although some peak values differ slightly. The calm water resistance and free-surface elevation are also of sufficient accuracy.

Attention must be paid not only to the chosen grid but also to the time step which can have a significant influence on the resulting forces and the accuracy of the generated wave amplitude if chosen smaller than a certain limit.

Performing sea spectrum analysis to determine individual wave forces has its limits, since the magnitude of the force amplitudes partially differ from the individually determined force amplitudes. Nevertheless, a satisfactory agreement of the predicted force amplitudes for the individual waves can be achieved. Attention must be paid though to the accuracy of the Fourier analysis, as this has a strong influence on the results.

REFERENCES

[1] Hino, T., ed., 2005. The Proceedings of CFD Workshop Tokyo 2005.

[2] Menter, F. R., 1993. " Zonal Two Equation k-ω Turbulence Models for Areodynamic Flows ". *24th Fluid Dynamics Conference*.

[3] Jacobsen, N. G., Fuhrman, D. R., and Fredsøe, J., 2012. " A Wave Generation Toolbox for the Open-Source CFD Library: OpenFoam® ". *Int. J. Numerl. Meth. Fluids,* ***70***(9), pp. 1073–1088.

[4] Wilcox, D. C., 1993. *Turbulence Modeling for CFD*. DCW Industries, La Cañada, California, USA.

[5] ITTC, 2008. Uncertainty Analysis in CFD Verification and Validation - Methodology and Procedures. Tech. rep., International Towing Tank Comference.

[6] Cura Hochbaum, A., and Pierzynski, M., 2005. "Flow Simulation for a Combatant in Head Waves". *The Proceedings of CFD Workshop Tokyo 2005*.